Published in final edited form as:
Biochemistry. 2013 July 9; 52(27): . doi:10.1021/bi4004364.

Magnesium impacts myosin V motor activity by altering key conformational changes in the mechanochemical cycle

Darshan Trivedi[1], **Joseph M. Muretta**[2], **Anja M. Swenson**[1], **David D. Thomas**[2], and **Christopher M. Yengo**[1,*]

[1]Department of Cellular and Molecular Physiology, College of Medicine, Pennsylvania State University, Hershey, PA 17033

[2]Department of Biochemistry, School of Medicine, University of Minnesota, Minneapolis, MN

Abstract

We investigated how magnesium (Mg) impacts key conformational changes during the ADP binding/release steps in myosin V and how these alterations impact the actomyosin mechanochemical cycle. The conformation of the nucleotide binding pocket was examined with our established FRET system in which myosin V labeled with FlAsH in the upper 50 kDa domain participates in energy transfer with *mant* labeled nucleotides. We examined the maximum actin-activated ATPase activity of MV FlAsH at a range of free Mg concentrations (0.1–9 mM) and find that the highest activity occurs at low Mg (0.1–0.3 mM), while there is a 50–60% reduction in activity at high Mg (3–9 mM). The motor activity examined with the *in vitro* motility assay followed a similar Mg-dependence and the trend was similar with dimeric myosin V. Transient kinetic FRET studies of *mant*dADP binding/release from actomyosin V FlAsH demonstrate that the transition between the weak and strong actomyosin. ADP states is coupled to movement of the upper 50 kDa domain and is dependent on Mg with the strong state stabilized by Mg. We find that the kinetics of the upper 50 kDa conformational change monitored by FRET correlates well with the ATPase and motility results over a wide range of Mg concentrations. Our results suggest the conformation of the upper 50 kDa domain is highly dynamic in the Mg free actomyosin. ADP state, which is in agreement with ADP binding being entropy driven in the absence of Mg. Overall, our results demonstrate that Mg is a key factor in coupling the nucleotide- and actin-binding regions. In addition, Mg concentrations in the physiological range can alter the structural transition that limits ADP dissociation from actomyosin V, which explains the impact of Mg on actin-activated ATPase activity and *in vitro* motility.

Keywords

Myosin; actin; FRET

The family of P-loop nucleotide triphosphatases (NTPases) which includes G-proteins, kinesins, and myosins contain a highly conserved and well characterized nucleotide binding region [1–3]. A common thread within this protein family is that the nucleotide bound to the activesite modulates the affinity of the NTPase for its track in the case of motors or effector protein in the case of G proteins [1, 2]. In motor proteins conformational changes in the active-site are also coupled to structural changes that produce force and motion. Three main structural elements are known to coordinate nucleotide binding and hydrolysis in the active-site of P-loop NTPases; P-loop, switch I, and switch II[4]. These elements coordinate an

*To whom correspondence should be addressed: Christopher M. Yengo, Department of Cellular and Molecular Physiology, College of Medicine, Pennsylvania State University, Hershey, PA 17033, USA, Tel.: (717) 531-8575; cmy11@psu.edu.

active-site magnesium ion (Mg) associated with the bound nucleotide that is thought to be central to high-affinity nucleotide binding and hydrolysis [5]. Studies with myosins have demonstrated that variations in physiological Mg concentrations can modulate motor activity [6–8]. In addition, coordination of the active-site Mg is also critical for the motor activity of kinesin suggesting a common structural mechanism may exist between these two motor protein families [9]. In G-proteins, Mg exclusion plays a critical role in mediating GDP dissociation [10–12]. In order to fully understand the potential role of metal-ion regulation in P loop NTPases it is critical to determine how Mg regulates key structural changes in their NTPase cycles.

Myosin motors generate force by coupling small conformational changes in the nucleotide binding region to a large swing of the light chain binding region ("lever arm") during a cyclic interaction with actin filaments. The actomyosin ATPase cycle (scheme 1) consists of nucleotide-states that correspond to either "weak" (bold) or "strong" actin binding conformations. In the absence of nucleotide myosin binds to actin with very high-affinity. ATP binding to actomyosin ($K'_1K'_2$) induces dissociation of the complex and the following ATP hydrolysis step (K_3) stabilizes the pre-force generating conformation. The hydrolysis products are released slowly from the active-site of myosin until actin binding accelerates the release of phosphate (K'_4) and triggers the force generating conformational change in the lever arm. The resulting actomyosin. ADP states have high actin affinity. The release of ADP is thought to occur in two steps, with the first step associated with an isomerization of the nucleotide binding pocket (NBP) (K_{5A} or K_{pocket}) and the second step involving local active-site rearrangements during the release of ADP (K_{5B} or K_{ligand}) [5–8, 13]. The active site isomerization is thought to be associated with a transition from a "weak" ADP affinity state to "strong" ADP affinity state [7]. An additional swing of the lever arm is thought to occur in many myosins during one or both of the ADP release steps [13–15].

Mg is required for ATP to bind to myosin with high-affinity and for the ATP hydrolysis step [16]. However, these steps are not likely important in altering the *in vivo* actomyosin motility as Mg concentrations in the physiological range (0.8–1.2 mM free Mg,[17]) do not significantly alter these steps. One common theme in the myosin motor family is that the ADP release step is critically important in mediating the contractile velocity and load dependence. Strain dependent ADP release limits the maximal sliding velocity of skeletal muscle myosin [18, 19] and allows for mechanical gating and processive walking of dimeric myosin V [20].

Several biochemical and structural studies have demonstrated that Mg can alter the kinetics of ADP release in myosin I, II, and V [6, 7, 21]. A study by Kintses et. al.[22] found that Mg shifts the equilibrium from the weak to the strong ADP binding state of Dictostelium myosin II. However, they could not determine if Mg was required to form the strong ADP binding conformation as is known to be the case in G-proteins [12]. Previous studies with myosin V have been particularly revealing in examining the actomyosin. ADP states and Mg dependence. Two studies examined the *mant*ADP fluorescence in the active site, which provided evidence for two ADP states in the presence and absence of actin[6, 7]. These studies found that Mg can impact the equilibrium between the weak and strong ADP states[6], as well as the rate of nucleotide release from the weak state [6, 7]. The results were in agreement with the crystal structure of myosin V in the presence of ADP, which contains no active site Mg and suggested Mg can be released from the active site prior to ADP[5]. Based on these results, Rosenfeld et al. [6]predicted varying free Mg concentrations would alter the motile properties of myosin V. Nagy et al.[8] followed up on these studies by demonstrating that free Mg can alter the actin-activated ATPase rate, which correlated with the overall rate of ADP release. Nagy et al.[8] also determined that mutating a residue associated with Mg coordination in the active site can impact the Mg dependence, suggesting that the Mg in the active site and not

another allosteric binding site is responsible for altering ADP release kinetics. However, no studies have directly correlated the actin-activated ATPase rate, *in vitro* motility, and specific structural transitions in the actomyosin. ADP states. Furthermore, it is unknown how Mg alters the structural transitions at the active site and how these transitions impact the conformation of functionally important regions of myosin, such as the actin-binding and lever arm regions.

We have developed a spectroscopic approach to examine structural changes in the actomyosin V. ADP states using FRET between *mant* labeled nucleotides and FlAsH labeled in the upper 50 kDa (U50) domain[23–25]. Our results are consistent with the FRET measurements being sensitive to the two structural actomyosin. ADP states, which we suggested to be modulated by the conformation of switch I[23, 24]. We determined that the equilibrium between the two switch I conformations in the presence of ADP is sensitive to temperature, since a shorter average distance was found at low temperature and a longer average distance was found at higher temperatures. Based on these results we hypothesize that the position of the U50 domain correlates with the position of switch I, and that the switch I movement may be coupled to the movement of the U50 domain. Communication between switch I and the U50 domain is thought to be responsible for ATP-induced dissociation of actomyosin as ATP binding induces a switch I closed/actin binding cleft open state with weak affinity for actin. We also found that mutations in the switch II region can impact the equilibrium between the two switch I conformations in the presence of ADP[24]. In the current study we examined the impact of Mg on specific structural transitions in the active site and how Mg alters the dynamics of the U50 domain. We also determined how Mg alters the kinetics and thermodynamics of structural changes associated with the actomyosin ADP release steps. Finally, we correlated the Mg dependence of the ADP release steps with the actin-activated ATPase and in vitro motility properties of myosin V. Our results demonstrate that Mg is a key factor in mediating the structural and chemo-mechanical properties of myosin V.

EXPERIMENTAL PROCEDURES

All reagents were of the highest purity commercially available. ATP and ADP were prepared fresh from powder. N-Methylanthraniloyl (*mant*)-labeled 2′-deoxy-ADP (*mant*dADP) was purchased from Jena Bioscience (Jena, Germany). The *mant*dADP concentration was determined from absorbance measurements at 255 nm using ε_{255} of 23,300 $M^{-1}\cdot cm^{-1}$. ATP and ADP concentrations were determined by absorbance at 259 nm using an ε_{259} of 15,400 $M^{-1}\cdot cm^{-1}$. FlAsH (fluorescein biarscenical hairpin-binding dye) was generously provided by Roger Tsien and Stephen Adams (University of California, San Diego).

Myosin V cDNA Construction, Expression, and Purification

Two chicken myosin V constructs were used for this study. One contained a single IQ motif (MV) (residues 1–792) and the other was a heavy meromyosin (MV HMM) construct containing an N-terminal FLAG tag and C-terminal YFP [26]. In the MV 1IQ construct residues 292–297 were substituted with a tetracysteine motif (Cys-Cys-Pro-Gly-Cys-Cys) for FlAsH labeling[23–25, 27]. MV contained a C-terminal Myc tag (EQKLISEEDL) followed by a FLAG tag (DYKDDDDK). The G440A mutation was introduced as described previously [24]. Both myosin V constructs were coexpressed with chicken calmodulin and purified by anti-FLAG affinity chromatography. The purity was greater than 95% based on Coomassie-stained SDS gels. Myosin concentrations were determined using the Bio-Rad microplate assay using bovine serum albumin (BSA) as a standard or by absorbance (ε_{280} = 103,600 $M^{-1}\cdot cm^{-1}$). MV labeled with FlAsH, referred to as MV FlAsH, was generated as

previously described [23–25, 27]. Actin was purified from rabbit skeletal muscle using an acetone powder method [28]. All experiments were performed in K50TCEP buffer (50 mM KCl, 1 mM EGTA, 1 mM TCEP, and 10 mM imidazole-HCl, pH 7.0, 25°C) supplemented with the appropriate amount of $MgCl_2$. Free Mg concentrations were calculated using MaxC 2.5 and the stability constants for ADP and ATP (http://www.stanford.edu~cpatton/).

Stopped-flow Measurements and Kinetic Modeling

Transient kinetic experiments were performed in an Applied Photophysics (Surrey, UK) stopped-flow apparatus with a dead time of 1.2 ms. A monochromator with a 2-nm band pass was used for fluorescence excitation, and cutoff filters were used to measure the fluorescence emission. All optical filters were provided with the stopped-flow instrument. The *mant*dADP was excited at 365 nm, in the presence and absence of MV FlAsH or unlabeled MV, and the FRET emission was measured with a 515 nm long pass filter. Nonlinear least-squares fitting of the data was done with software provided with the instrument or Kaleidagraph (Synergy Software, Reading, PA). Uncertainties reported are standard error of the fits unless stated otherwise. All concentrations mentioned in the stopped-flow experiments are final concentrations unless stated otherwise.

Kinetic modeling and simulations were performed with Pro-K (Applied Photophysics) or Kintek Explorer (Kintek Corp.) software using schemes 1 and 2, also used in kinetics studies of myosin V [6, 7, 23, 24]. The *mant*dADP binding and dissociation transients were normalized prior to fitting to the kinetic model. The *mant*dADP binding data were fit to a two-step binding model described in previous reports [7, 23, 29], where the slow and fast exponential rates, and the amplitude of the slow phase from the double exponential fits are described by equations 1–3. The equation (Eq. 3) defining the amplitude of the slow phase was slightly modified from our previous report [23], since the component associated with the unbound *mant*dADP does not contribute to the fluorescence enhancement.

$$k_{\text{slow}}=\frac{(k_{+\text{ligand}}*[\text{mantdADP}](k_{-\text{pocket}}+k_{+\text{pocket}})+k_{-\text{ligand}}*k_{+\text{pocket}})}{(k_{+\text{ligand}}*[\text{mantdADP}]+k_{-\text{ligand}}+k_{+\text{pocket}}+k_{-\text{pocket}})} \quad \text{(Eq. 1)}$$

$$k_{\text{fast}}=k_{+\text{ligand}}*[\text{mantdADP}]+k_{-\text{ligand}}+k_{+\text{pocket}}+k_{-\text{pocket}} \quad \text{(Eq. 2)}$$

where $k_{+\text{ligand}}$ was determined from the linear dependence of *mant*dADP binding to actomyosin V (fast phase of *mant*dADP binding to actomyosin).

$$A_{\text{slow}}=(k_{+\text{pocket}}/k_{-\text{pocket}})/(1+k_{+\text{pocket}}/k_{-\text{pocket}}) \quad \text{(Eq. 3)}$$

The *mant*dADP dissociation transients were also fit to a two state model described by Hannemann *et al.*[7] and used in our previous report [23]. Equations 4–6 were used to describe the fast and slow exponential rate constants, as well as the amplitude of the slow phase of the double exponential transient.

$$k_{\text{fast}}=k_{-\text{ligand}}+k_{+\text{pocket}} \quad \text{(Eq. 4)}$$

$$k_{\text{slow}}=k_{-\text{pocket}}[k_{-\text{ligand}}/(k_{-\text{ligand}}+k_{+\text{pocket}})] \quad \text{(Eq. 5)}$$

$$A_{\text{fast}}=[k_{-\text{pocket}}/(k_{+\text{pocket}}+k_{-\text{pocket}})]*[k_{-\text{ligand}}/(k_{-\text{ligand}}+k_{+\text{ligand}})] \quad \text{(Eq. 6)}$$

The overall affinity can be calculated with equation 7.

$$K_D = 1/K_{\text{ligand}} * \{(1/K_{\text{pocket}})/[1+(1/K_{\text{pocket}})]\} \quad \text{(Eq. 7)}$$

Thermodynamic analysis

The thermodynamic parameters were determined by examining the temperature dependence of each of the ADP-binding steps as described [23]. The enthalpic and entropic contributions to the free-energy associated with each step were calculated in the presence of 2 mM and 10 mM $MgCl_2$ as well as 4 mM EDTA.

FRET Measurements

FRET was used to measure the distance between donor fluorophore, *mant*dADP, and the acceptor fluorophore, FlAsH-labeled MV, using the Förster energy transfer theory [23]. The energy transfer efficiency (E) was measured from the increase in acceptor emission. We mixed acto-MV FlAsH with *mant*dADP (donor *mant*dADP+ acceptor), acto-MV unlabeled with *mant*dADP (donor only), and acto-MV FlAsH and ADP (acceptor only) and monitored the stopped-flow fluorescence (excitation 365 nm) transients with a 515 nm long pass filter. The efficiency of energy transfer and distance between the donor and acceptor probes was calculated using equations described in our previous work [23–25, 27]. The only difference from our previous work was that we used the fluorescence intensity determined from the stopped-flow mixing transients instead of the fluorescence spectra examined in a spectrofluorimeter. We observed no difference in the quantum yield of *mant*dADP bound to actomyosin V in the presence and absence of Mg, while differences in the *mant*dADP quantum yield at different temperatures were taken into account as previously described [23, 24].

Time Resolved Anisotropy

Time-resolved anisotropy was measured using a custom built single-photon counting (SPC) spectrophotometer [30]. The G-factor for this instrument is 1.0. Polarized time-resolved fluorescence waveforms were acquired with the emission polarizer orientation set to 0°, 54.7°, and 90° relative to the vertically polarized excitation source and analyzed globally according to Eq 8–12 [31]. The observed fluorescence, I(t), is fit by convolving the measured instrument response function, IRF, determined from light scatter of the excitation source, with the polarization-dependent fluorescence decay function, f(pol, t) (Eq. 8). The polarized fluorescence decay model depends on the emission polarization with the magic-angle emission (54.7°, Eq. 9) described by a sum of exponentials with discrete amplitude, A_i, and lifetime, τ_i, terms. The vertically (0°) and horizontally (90°) polarized emissions depend on the magic-angle emission and the time-resolved anisotropy function, r(t), according to Eq. 10 and 11. The time-resolved anisotropy function was assumed to be a single exponential with initial, r_i, and infinite, r_∞, anisotropies, and rotational correlation time, τ_{Ri} (Eq. 12). The initial anisotropy, r_i, infinite anisotropy, r_∞, and rotational correlation time, τ_{Ri}, were global parameters shared by all lifetime species τ_i in Eq. 9. The total anisotropy was calculated from the time-resolved fluorescence, and time-resolved anisotropy functions according to Eq. 13.

$$I(t) = \int_{-\infty}^{\infty} \text{IRF}(t-t') f_{(\text{pol},t)}(t') dt \quad \text{(Eq. 8)}$$

$$f(54.7^\circ,t)=\sum_{i=1}^{2} A_i e^{-\frac{t}{\tau_i}} \quad \text{(Eq. 9)}$$

$$f(0^\circ,t)=(1/3)f(54.7^\circ,t)[1+2r(t)] \quad \text{(Eq. 10)}$$

$$f(90^\circ,t)=(1/3)f(54.7^\circ,t)[1-2r(t)] \quad \text{(Eq. 11)}$$

$$r(t)=r_\infty+r_i\exp(-t/\tau_{\mathrm{Ri}}) \quad \text{(Eq. 12)}$$

$$r_o=\frac{\int_{-\infty}^{\infty} f(54.7^\circ t)r(t)dt}{\int_{-\infty}^{\infty} f(54.7^{\circ\prime}t)dt} \quad \text{(Eq. 13)}$$

Mg Dependence of ADP release rate constants

We used the equation described in Rosenfeld et al.[6] to determine the Mg affinity for acto-MV FlAsH in the weak and strong ADP binding states. This equation also allows for extrapolating the ADP release rate constants to Mg free and saturating conditions,

$$k_{-\mathrm{pocket.Obs}}=\frac{k_{-\mathrm{Mg\ \ pocket}} * ([\mathrm{Mg}]/K_{D.\mathrm{Mg}})+k_{-\mathrm{pocket}}}{([\mathrm{Mg}]/K_{D.\mathrm{Mg}})+1} \quad \text{(Eq. 14)}$$

where $k_{-\mathrm{pocket.obs}}$ is the rate constant determined at each Mg concentration, $k_{-\mathrm{pocket}}$ is the rate constant extrapolated to Mg free conditions, and $k_{-\mathrm{Mg.pocket}}$ is the rate constant at saturating Mg conditions, [Mg] is the free Mg concentration, and $K_{\mathrm{D.Mg}}$ is the affinity of Mg for the actomyosin. ADP strong state. A similar analysis was performed with the $k_{-\mathrm{ligand}}$ rate constant.

ATPase Assays

ATPase assays were performed in the stopped-flow at 25°C using the NADH coupled assay [25, 32]. The steady-state ATPase rate at each Mg concentration (0.5–10 mM $MgCl_2$) of 0.05–0.1 μM MV FlAsH or MV HMM in the presence of 20 μM actin and 1 mM ATP was determined.

In Vitro Motility Assays

Actin filament motility was measured using the *in vitro* motility assay [33] used previously to measure MV FlAsH [25] and MV HMM [26] motility. MV FlAsH was specifically attached to the nitrocellulose-coated surface with an anti-Myc antibody, while MV HMM was directly adhered to the nitrocellulose-coated surface. The surface was blocked with bovine serum albumin at a concentration of 1 mg/ml. The motility of F-actin labeled with rhodamine-phalloidin was observed using an activation buffer consisting of K50 supplemented with the appropriate amount of Mg, 3.4 μM calmodulin, 0.35% methylcellulose, and 1 mM ATP. Phosphoenol pyruvate (2.5 mM) and pyruvate kinase (20 units/ml) were added as an ATP regeneration system. Glucose oxidase (0.1 mg/ml), glucose (3 mg/ml), and catalase (0.018 mg/ml) were added to reduce photobleaching. After the addition of the activation buffer, the slide was promptly viewed using a NIKON TE2000 microscope equipped with a 60x/1.4NA phase objective. Images were acquired at 2–5 second intervals for a period of 3–5 minutes. We utilized a shutter controlled Coolsnap HQ2 cooled CCD digital camera (Photometrics)

binned 2x2 for all imaging. To measure velocity, the video records were transferred to Image J and analyzed with the MtrackJ program [34].

RESULTS

Mg alters steady-state ATPase and in vitro motility

We examined the steady-state ATPase activity of MV FlAsH (Figure 1A) and MV HMM (Figure 1B) in the presence of 20 μM actin using the NADH coupled assay at 25°C. The ATPase activity was measured with K50 buffer containing varying concentrations of $MgCl_2$ (0.5, 1.0, 2.0, 4.0, 6.0, 8.0, 10.0 mM). The actin-activated ATPase results were plotted as a function of free Mg concentration. We found that the highest ATPase activities were observed at low free Mg concentrations (0.1–0.3 mM) and there was a 60% reduction in activity at high free Mg concentrations (3–9 mM). We also examined the sliding velocity with MV FlAsH (Figure 1A) and MV HMM (Figure 1B) in the *in vitro* motility assay and found the Mg-dependence was very similar to the ATPase results (Figure 1). We analyzed 20–30 filaments per condition and the mean and standard error of the mean was calculated for each Mg concentration. In K50 buffer containing 4 mM EDTA, there was no actin-activated ATPase activity (rate = 0.06 s^{-1}) or *in vitro* motility observed.

mantdADP binding to acto-MV FlAsH with and without Mg

We examined the impact of Mg on the conformational changes associated with ADP binding to acto-MV. The kinetics of nucleotide binding were examined by mixing *mant*dADP with acto-MV FlAsH in the stopped-flow at 4, 10, 15, and 25°C in K50 buffer with 2 mM $MgCl_2$ or 4 mM EDTA (Figure 2). The FRET signal was examined by exciting at 365 nm and measuring the fluorescence emission through a 515 nm long pass filter. In the presence of 2 mM $MgCl_2$, the fluorescence transients were best fit to a bi-exponential function. The fast phase was found to be linearly dependent on *mant*dADP concentrations (Figure 2A) while the slow phase was independent of *mant*dADP concentrations (Figure 2B). Thus, the data were fit to a kinetic model described previously [23], in which *mant*dADP first forms a “weak or open” (K_{ligand}) complex with actomyosin and transitions into a “strong or closed” (K_{pocket}) conformation (scheme 2). The slope of the linear dependent fast phase was used to determine $k_{+ligand}$ and the transients were fit to kinetic equations 1–3 to determine $k_{+pocket}$, $k_{-pocket}$, and $k_{-ligand}$ (scheme 2)

The fast and slow phases of *mant*dADP binding to acto-MV FlAsH were both dependent on temperature. The relative amplitudes of the fast and slow components were similar over the range of *mant*dADP concentrations measured but varied at each temperature (Figure 2D). Overall, our kinetic results from *mant*dADP binding to acto-MV FlAsH in the presence of 2 mM $MgCl_2$ were similar to our previous results with 1 mM $MgCl_2$ [23] except the relative amplitudes demonstrated a higher fractional distribution of the slow component. Identical experiments were performed in the presence of 10 mM $MgCl_2$ and the rates and relative amplitudes of the fast and slow components were similar to 2 mM $MgCl_2$ (Table 1). These results indicate that the strong ADP conformation and corresponding “high-FRET” position of the U50 domain is more favorable at higher $MgCl_2$ concentrations. Under Mg free conditions (4 mM EDTA K50 buffer) we found that the fluorescence transients were dominated by a fast fluorescence increase that fit to a single exponential and was linearly dependent on the *mant*dADP concentrations (Figure 2C). The second-order rate constant determined from the slope of the single exponential fits as a function of *mant*dADP concentrations was faster than determined with Mg, especially at 25°C where it was more than 2-fold faster (Figure 2C, Table 1). The y-intercept of the linear fit of the fast component was about 10-fold higher without Mg than in the presence of 2 mM $MgCl_2$.

Conformation of the nucleotide binding pocket as a function of temperature with and without Mg

We determined the maximum FRET efficiency of the acto-MV FlAsH.*mant*dADP complex by stopped-flow mixing and measurement of acceptor enhancement (Figure 3). Compared to conventional titrations, stopped flow mixing reduces inner filter effects arising at high *mant*dADP concentrations and at the same time yields fluorescence transients from which amplitudes and kinetic rates can be determined.

We determined the amplitude of the FRET signal in the stopped-flow after mixing acto-MV FlAsH (0.5 μM actin, 0.25 μM MV FlAsH) with varying concentrations of *mant*dADP (0–30 μM *mant*dADP) in the presence of 2 mM $MgCl_2$ (Figure 3A) or 4 mM EDTA (Figure 3C) at 4, 15, and 25°C. The amplitudes of the donor only and acceptor only were also determined at 30 μM *mant*dADP concentration, which allowed for determination of the FRET efficiency and calculated distances, as summarized in Table 2. In the current study, the trend of distance change as a function of temperature at 2mM $MgCl_2$ was similar to our previous work at 1mM $MgCl_2$ [23]. (The distance change is 4.5Å at 2mM $MgCl_2$ and 2–4Å at 1mM $MgCl_2$ [23]).

At low temperature (4°C) we found the average distance was similar in the presence (2 mM $MgCl_2$) and absence of Mg (4 mM EDTA). Interestingly, at 25°C the FRET distance increased dramatically in the absence of Mg, while in the presence of Mg there was a much smaller increase in distance relative to 4°C. Therefore, the temperature-dependent change in FRET is much more dramatic in the absence of Mg.

Dissociation of mantdADP from acto-MV FlAsH with and without Mg

We examined *mant*dADP dissociation from acto-MV FlAsH in K50 buffer containing 2 mM $MgCl_2$ and 4 mM EDTA (Figure 4). A complex of acto-MV FlAsH.*mant*dADP was mixed with saturating ATP (final concentrations: 0.25 μM MV FlAsH, 0.5 μM actin, 10 μM *mant*dADP, 1 mM ATP) and the resulting fluorescence decrease was monitored as described above (ex = 365 nm, em = 515 nm long pass filter). As observed in our previous work [23] the fluorescence transients followed a biexponential function in the presence of Mg (Figure 4A and C). The fast component was equivalent to the y-intercept from the *mant*dADP binding experiments (Figure 2), and therefore the slow component was modeled to be the conformational change in the U50 domain associated with the transition from the “strong” to “weak” actomyosin. ADP nucleotide state. We fit the fluorescence transients to kinetic equations 1–6 defined previously [7] and used in our previous report [23], which allowed us to determine rate constants $k_{-pocket}$, $k_{+pocket}$, $k_{-ligand}$ at each temperature. The values for these rate constants are reported as the average from the association and dissociation experiments (Table 1), demonstrating relatively good consistency between both sets of experiments. The fluorescence transients were also fit to kinetic schemes using Kintek explorer and the fits yielded rate constants that matched well with fits performed using analytical equations. The fluorescence transients in the absence of Mg (4 mM EDTA) were dominated by a fast fluorescence decrease that was ~10-fold faster than in the presence of Mg (Figure 4B). We observed a slow fluorescence decrease (~0.5 s^{-1}) that was a small component of the total fluorescence change (~5%) at lower temperatures (4–15°C). We attribute the slow transition to an off-pathway intermediate since the predicted rate constant for $k_{-pocket}$ in the absence of Mg is much faster (14.8±0.2 s^{-1}) (see Figure 6B). The slow fluorescence decrease could also be due to non-specific interactions of *mant*dADP and MV FlAsH.

Mg concentration dependence of mantdADP release from acto-MV FlAsH

We examined conformational changes in acto-MV FlAsH during *mant*dADP release as described above in the presence of the entire range of Mg concentrations (0.5 – 10 mM

$MgCl_2$) at 25°C (Figure 5). A complex of acto-MV FlAsH.*mant*dADP was mixed with saturating ATP (final concentrations: 0.25 μM MV FlAsH, 0.5 μM actin, 10 μM *mant*dADP, 1 mM ATP) in K50 buffer containing differing amounts of $MgCl_2$. The fluorescence transients of the FRET signal were fit to a bi-exponential function at all Mg concentrations (Figure 5A & C). We found that the fast phase and slow phases of *mant*dADP release were both altered by Mg concentration, with the fast phase more steeply dependent on Mg. The relative amplitudes of the fast and slow phases were also dependent on Mg, with the fast phase more populated at low Mg concentrations and the fast/slow amplitude distribution similar at free Mg concentrations 0.9 mM and above. We determined the rate constants $k_{-pocket}$, $k_{+pocket}$, $k_{-ligand}$ at each Mg concentration (25°C) as described above (Figure 6 A & B).

To examine the role of the switch II region in Mg-dependent ADP release, similar experiments were performed with the mutant MV^{G440A} FlAsH [24] in the presence of actin. The G440A mutation disrupts the rotation of switch II which prevents closure of the NBP and uncouples the nucleotide and actin binding regions in myosin V [13]. The fluorescence transients of *mant*dADP release from MV^{G440A} FlAsH showed two phases, while the slow phase was 10-fold slower than wild-type MV FlAsH (Figure 5 B & D). It is unclear if the slow phase represents the strong-to-weak ADP transition, an off pathway intermediate, or non-specific interactions. The release from the weak actomyosin. ADP ($k_{-ligand}$) state was similar to wild-type in the absence of Mg but was accelerated 3-fold at saturating Mg. Thus, the ability of Mg to slow the rate constant for ADP release from the weak state is attenuated in MV^{G440A} FlAsH.

Correlation of the strong-to-weak ADP isomerization with the maximum ATPase rate

Kinetic analysis allowed for determination of the rate and equilibrium constants associated with the formation of the weak actomyosin. ADP state (K_{ligand}) and transition into the strong actomyosin. ADP state (K_{pocket}) [7, 23]. Figure 6A demonstrates the dependence of K_{pocket} on the Mg concentration which increases to a value of 0.33 at 0.9 mM free Mg and above. The ADP release rate constant for myosin V was found to be similar with *mant*dADP and unlabeled ADP [32, 35] and this is the rate limiting step in the actin-activated ATPase[35] and *in vitro* motility[36] assays. Therefore, it is reasonable to examine the correlation between the steady-state assays (Figure 1) done with unlabeled ATP to the transient kinetic results performed with *mant*dADP. A comparison of the $k_{-pocket}$ rate constant and the k_{cat} for ATPase as a function of Mg demonstrates these rates are very similar in the range of $MgCl_2$ concentrations analyzed (0.5 – 10 mM). We also demonstrate that $k_{-ligand}$ is at least two-fold faster than $k_{-pocket}$ in this Mg concentration range (Figure 6B). Our results demonstrate that the $k_{-pocket}$ step correlates well with the rate limiting step in the ATPase cycle which we also concluded from our temperature dependent studies [23]. By fitting the Mg dependence of $k_{-pocket}$ to the equation (Eq. 14) described by Rosenfeld et al. [6] we determined the value of $k_{-pocket}$ in the absence of Mg ($k_{-pocket}$ = 14.8 ± 2.0). This equation also allows estimation of the Mg affinity in the actomyosin V strong ($K_{D.Mg}$ = 0.9 ± 0.4 mM) and weak ($K_{D.Mg}$ = 0.6 ± 0.3 mM) ADP binding conformations, while the affinity of Mg for free ADP (K_D = 0.35±0.3 mM) was previously determined[7]. By the principle of detailed balance, the value for K_{pocket} and $k_{+pocket}$ in the absence of Mg was estimated to be 0.28 and 4.2 s^{-1}, respectively. The estimated values for K_{pocket} and $k_{+pocket}$ are not in agreement with our results that demonstrate the slow phase was not present in the dissociation and binding experiments. Thus, it is likely that there are multiple biochemical states in the absence of Mg.

Thermodynamic analysis

The thermodynamic parameters associated with the K_{ligand} and K_{pocket} steps were calculated from the van't Hoff plots (Figure 6C and Table 3). It should be noted that the values for K_{ligand} are reported under standard state conditions (1M concentration of reactants) and therefore the value for $k_{+ligand}$ is likely an overestimate. In addition, previous studies demonstrated that K_{ligand} inlcudes two steps, the formation of the collision complex between actomyosin and *mant*dADP followed by the transition into the weak actomyosin. ADP state[7, 37]. Therefore, the calculated free energy values for K_{ligand} should be interpreted as a relative comparison, while the thermodynamic analysis provides information about the role of Mg in this biochemical transition. The free energy change associated with K_{ligand} in the presence of Mg was dominated by the enthalpic component in the presence of 2 and 10 mM $MgCl_2$. Interestingly, in the absence of Mg (4 mM EDTA) we found that the enthalpic component was dramatically reduced while there was a large positive entropic component associated ADP binding. We found that the thermodynamics of the K_{pocket} step were entropy driven and quite similar at 2 and 10 mM $MgCl_2$, as well as similar to our previous measurements at 1 mM $MgCl_2$[23].

Time-resolved anisotropy

The time-resolved anisotropy measurements demonstrate that the FlAsH fluorophore has a rotational correlation time on the ns time scale (Table 4). There results suggest that although the FlAsH fluorophore is fairly restricted in is dynamics because of its attachment to the tetracysteine motif, it has some dynamic motion that will randomize the orientation factor. We also determined that there was no difference in the time-resolved anisotropy parameters in comparing the acto-MV. ADP and acto. MV states, which suggest the local environment of the FlAsH fluorophore does not change in the strong and weak ADP binding states.

DISCUSSION

Many studies have focused on the ADP release steps of the actomyosin ATPase cycle, as these steps have been linked to strain dependent processive walking in myosin V [38, 39] and the detachment limited model of muscle contraction in myosin II [19]. The current study focuses on how Mg impacts the structural changes associated with the ADP release steps in actomyosin V. We find that the actin-activated ATPase and motile properties of both monomeric and dimeric myosin V are similarly dependent on Mg. We demonstrate that high Mg impacts ADP release by slowing the rate-limiting isomerization of the NBP, which is associated with movement of the U50 domain. Additionally, we find that the release of ADP from the "weak" ADP affinity state is Mg dependent as was reported previously [6, 7]. FRET results indicate a more dramatic temperature dependent distance change in the absence of Mg, suggesting Mg is essential for stabilizing the "strong" ADP affinity conformation. Overall, our results indicate that active-site Mg coordination can impact key structural changes that are critical for the motile and force generating properties of myosin V.

Structural mechanism of MgADP coordination in myosin V

Mg is coordinated in the NBP with highly conserved structural elements. S218 of switch I and T170 of the P-loop coordinate Mg directly while D437 of switch II coordinates the Mg via a water molecule [5] (Figure 7). Our results suggest Mg coordination by these structural elements is likely important for stabilizing the "strong" ADP affinity NBP conformation. It has been proposed that strong actin binding causes switch I to favor an open conformation, which perturbs the coordination of Mg and initiates structural rearrangements that lead to the release of ADP [22]. The crystal structure of myosin V in the presence of ADP has no Mg present and both switch I and II adopt an open conformation [5]. Such an active-site conformation is also seen in the crystal structure of nucleotide free myosin V, which fits

well into to the rigor actomyosin complex determined by cryo-electron microscopy [40]. Our results show that the conformation of the U50 domain, which is proposed to be dependent on the position of switch I [23], is in turn dependent on Mg. Our previous work has demonstrated that switch II also plays a role in stabilizing a closed NBP conformation and is involved in the allosteric communication between the nucleotide and actin binding regions [24]. Nagy et al [8] found that mutations in switch II can disrupt the Mg dependent ADP release mechanism. Our results further demonstrate the role of switch II in ADP release, since the G440A mutant [41] disrupts formation of the strong ADP affinity state even at 10 mM $MgCl_2$ (Figure 5B&D). Because the G440A mutation prevents a closed switch II conformation it may indirectly impact the coordination of Mg by preventing D437 of switch II from properly coordinating Mg through a water molecule. Moreover, the G440A mutation may also impact the hydrogen bond between Y439 of switch II and R219 of switch I [8] that could potentially alter the direct Mg coordination by S218 of switch I (Figure 7). Also, in kinesin the interaction between switch I and switch II and their coordination of Mg and surrounding water molecules is critical for Mg and ADP release. Switch II in kinesins has been shown to undergo a large movement during Mg release [42]. Since the G440A mutation precludes the rotation of switch II, we expected a complete insensitivity to Mg in the ADP dissociation experiments (Figure 5B&D). However, we only see a partial insensitivity, and we attribute this observation to the fact that apart from the indirect coordination of Mg via switch II, Mg is also directly coordinated via residues of P-loop and switch I which may play a role in the modest suppression of ADP release at higher Mg in the G440A mutant. The current study and previous work[8, 24] that examined the impact of switch II mutations implies that the Mg-dependence of the structural changes we observe are attributed to Mg binding in the active site, while we cannot rule out that Mg binding to another allosteric site in myosin could alter key structural transitions.

Mg is required for formation of the strong ADP binding state

Our earlier work found that the strong-weak ADP binding equilibrium monitored by FRET is temperature dependent and provides an indication of the distance change associated with the two conformations [23]. Scheme 2 demonstrates the pathway for ADP release from actomyosin, which indicates the Mg free (lower) and Mg saturated (upper) pathways. In current study we investigated the impact of Mg on FRET as a function of temperature. In the presence of Mg, the kinetic studies fit well to Scheme 2 (top) in which K_{pocket} determines the population of the weak (low FRET) and strong (high FRET) ADP binding states. In the absence of Mg, the kinetic measurements of both *mant*dADP binding and release indicate that actomyosin V is dominated by a single conformation at all temperatures (Figures 2C, 3C&D, 4B&C). At lower temperatures the FRET distance in the presence and absence of Mg is similar, while at higher temperatures the difference dramatically increases (~5Å). These results can be explained if the weak ADP binding conformation is highly dynamic in the absence of Mg. This highly flexible state allows some high FRET conformations, relatively close distances between the mant-FlAsH fluorophores, to be populated on the nanosecond timescale even though the NBP is in a weak ADP binding conformation. The transitions into the high FRET conformations are not seen in the kinetic measurements because they are too rapid and ensemble averaged. Interestingly, the high FRET conformations are more populated at low temperature indicating the structure is more flexible at low temperature. It is possible that there is a hinge region that becomes more flexible at lower temperatures, similar to what is found in cold-denaturation [43–45]. As temperature increases in the absence of Mg the flexible region becomes more rigid and only the low FRET states are populated. The thermodynamic analysis supports the hypothesis that the weak ADP binding state is highly flexible in the absence of Mg. We find that ADP binding occurs with a large positive entropy, suggesting enhanced conformational entropy,

only in the absence of Mg. Hence, Mg coordination is required for formation of the strong ADP affinity state and may be coupled to the flexibility of the U50 domain.

Kinetic mechanism of Mg dependent ADP release

Two previous studies examined the influence of Mg on the kinetics of the ADP release steps in myosin V [6–8]. These studies examined the FRET signal from internal tryptophan residues to *mant*ADP or *mant*dADP. Our results are in good general agreement with these studies in that they concluded that Mg strongly influences the rate constant for ADP release from the weak ADP binding state [6, 7]. Our FRET results with the *mant*-FlAsH pair suggest that Mg coordination enhances the formation of the switch I closed NBP conformation, as originally proposed by Rosenfeld et al.[6]. In addition, our results demonstrate directly that the Mg dependent change in the NBP is coupled to the conformation of the U50 domain. Interestingly, Hannemann et al.[7] also found that there was a structural change in the actin binding region detected by a difference in the degree of pyrene actin quenching in the two actomyosin. ADP states. The probability of Mg being released prior to the release of the cation-free ADP species was also proposed by Rosenfeld et al. [6]. Our results are in agreement with Rosenfeld et al.[6] in that Mg exchange can occur in both the strong and weak ADP binding states, which allows Mg to influence both the K_{pocket} and K_{ligand} steps.

Our current results indicate that Mg can alter the rate-limiting conformational step wherein the NBP goes from a strong to weak ADP binding state ($k_{-pocket}$) prior to the release of ADP (Figure 6A). The maximal ATPase rate and *in vitro* motility sliding velocities as a function of Mg follow a similar trend as the $k_{-pocket}$ rate constant (Figures 1 & 6B). Therefore, our results favor a mechanism in which Mg can dissociate from the strong ADP binding state, which accelerates the transition into the weak ADP binding state ($k_{-pocket}$) and results in faster ADP release, maximal ATPase activity, and *in vitro* motility.

Implications for Mg dependent regulation of MV

Many enzymes and cellular functions are known to be dependent on Mg, the second most abundant cation in the cell. The concentration of Mg inside cells is tightly regulated while large fluxes of Mg across the cell membrane have been reported [17, 46]. The cytosolic free Mg levels are different in different cell types and they range between 0.8–1.2 mM. A recent *in vitro* study [47] with dynein demonstrated a reduction in its processivity at higher Mg concentrations while, at lower Mg concentrations, there was an enhancement in dynein processivity. This work speculated on the *in vivo* role of Mg as a switch to regulate the processivity of motor proteins like dynein. Our study shows significant changes in the functional properties of both monomeric and dimeric myosin V in the physiological Mg concentration range. The processive mechanism of dimeric myosin V is tightly coupled to strain sensitivity and mechanical gating between its two heads plays a critical role in this process. It is hypothesized that the ~50-fold difference in the rates of ADP release from the lead and trail heads of myosin V is associated with the pre- and post-powerstroke conformation of the lever arm [48, 49]. Mg may play an important role in a strain dependent communication pathway between the lever arm and the NBP which alters the ADP release rates in response to strain. Interestingly, a recent study found that in kinesin the metal ion binding site can be altered to allow manganese binding which allows the enzymatic and motile properties of kinesin to be modulated by the presence of manganese[9]. Therefore, understanding the mechanism of metal ion regulation of motor proteins could be utilized as a mechanism for specifically altering the *in vivo* activity of motors and for designing motor-based nanodevices. Future studies on myosin will focus on the impact of Mg on lever arm swing and its impact on strain dependent ADP release. Overall, the current study suggests a central role for Mg in mediating the force generating and motile activities of myosin V,

which provides a framework for revealing the conserved structural mechanism of the load dependent ADP release in myosin motors.

Acknowledgments

We thank William Unrath for outstanding technical assistance. We thank Jörg Rösgen and Don Jacobs for helpful discussions.

Funding Information: This work was supported by NIH grants (HL093531 and EY0181416) and a grant from the Pennsylvania Department of Health to CMY, a NIH grant (AR032961) to DDT and an American Heart Association pre-doctoral fellowship to DT.

Abbreviations

FRET	Fluorescence Resonance Energy Transfer
FlAsH	fluorescein biarscenical hairpin-binding dye
mant	N-methylanthraniloyl
***mant*dADP**	mant-labeled 2′-deoxy-ADP
TCEP	tris(2-carboxyethyl)phosphine hydrochloride

References

1. Vale RD. Switches, latches, and amplifiers: common themes of G proteins and molecular motors. J Cell Biol. 1996; 135:291–302. [PubMed: 8896589]
2. Kull FJ, Vale RD, Fletterick RJ. The case for a common ancestor: kinesin and myosin motor proteins and G proteins. J Muscle Res Cell Motil. 1998; 19:877–886. [PubMed: 10047987]
3. Goody RS, Hofmann-Goody W. Exchange factors, effectors, GAPs and motor proteins: common thermodynamic and kinetic principles for different functions. Eur Biophys J. 2002; 31:268–274. [PubMed: 12122473]
4. Smith CA, Rayment I. Active site comparisons highlight structural similarities between myosin and other P-loop proteins. Biophys J. 1996; 70:1590–1602. [PubMed: 8785318]
5. Coureux PD, Sweeney HL, Houdusse A. Three myosin V structures delineate essential features of chemo-mechanical transduction. EMBO J. 2004; 23:4527–4537. [PubMed: 15510214]
6. Rosenfeld SS, Houdusse A, Sweeney HL. Magnesium regulates ADP dissociation from myosin V. J Biol Chem. 2005; 280:6072–6079. [PubMed: 15579901]
7. Hannemann DE, Cao W, Olivares AO, Robblee JP, De La Cruz EM. Magnesium, ADP, and actin binding linkage of myosin V: evidence for multiple myosin V-ADP and actomyosin V-ADP states. Biochemistry. 2005; 44:8826–8840. [PubMed: 15952789]
8. Nagy NT, Sakamoto T, Takacs B, Gyimesi M, Hazai E, Bikadi Z, Sellers JR, Kovacs M. Functional adaptation of the switch-2 nucleotide sensor enables rapid processive translocation by myosin-5. FASEB J. 2010; 24:4480–4490. [PubMed: 20631329]
9. Cochran JC, Zhao YC, Wilcox DE, Kull FJ. A metal switch for controlling the activity of molecular motor proteins. Nat Struct Mol Biol. 2011; 19:122–127. [PubMed: 22198464]
10. Yang J, Zhang Z, Roe SM, Marshall CJ, Barford D. Activation of Rho GTPases by DOCK exchange factors is mediated by a nucleotide sensor. Science. 2009; 325:1398–1402. [PubMed: 19745154]
11. Hakoshima T, Shimizu T, Maesaki R. Structural basis of the Rho GTPase signaling. J Biochem. 2003; 134:327–331. [PubMed: 14561717]
12. Shimizu T, Ihara K, Maesaki R, Kuroda S, Kaibuchi K, Hakoshima T. An open conformation of switch I revealed by the crystal structure of a Mg2+-free form of RHOA complexed with GDP. Implications for the GDP/GTP exchange mechanism. J Biol Chem. 2000; 275:18311–18317. [PubMed: 10748207]

13. Veigel C, Coluccio LM, Jontes JD, Sparrow JC, Milligan RA, Molloy JE. The motor protein myosin-I produces its working stroke in two steps. Nature. 1999; 398:530–533. [PubMed: 10206648]
14. Veigel C, Molloy JE, Schmitz S, Kendrick-Jones J. Load-dependent kinetics of force production by smooth muscle myosin measured with optical tweezers. Nat Cell Biol. 2003; 5:980–986. [PubMed: 14578909]
15. Veigel C, Wang F, Bartoo ML, Sellers JR, Molloy JE. The gated gait of the processive molecular motor, myosin V. Nat Cell Biol. 2002; 4:59–65. [PubMed: 11740494]
16. Bagshaw CR, Eccleston JF, Eckstein F, Goody RS, Gutfreund H, Trentham DR. The magnesium ion-dependent adenosine triphosphatase of myosin. Two-step processes of adenosine triphosphate association and adenosine diphosphate dissociation. Biochem J. 1974; 141:351–364. [PubMed: 4281654]
17. Romani AM. Cellular magnesium homeostasis. Arch Biochem Biophys. 2011; 512:1–23. [PubMed: 21640700]
18. Nyitrai M, Rossi R, Adamek N, Pellegrino MA, Bottinelli R, Geeves MA. What limits the velocity of fast-skeletal muscle contraction in mammals? J Mol Biol. 2006; 355:432–442. [PubMed: 16325202]
19. Siemankowski RF, Wiseman MO, White HD. ADP dissociation from actomyosin subfragment 1 is sufficiently slow to limit the unloaded shortening velocity in vertebrate muscle. Proc Natl Acad Sci USA. 1985; 82:658–662. [PubMed: 3871943]
20. Nyitrai M, Geeves MA. Adenosine diphosphate and strain sensitivity in myosin motors. Philos Trans R Soc Lond B Biol Sci. 2004; 359:1867–1877. [PubMed: 15647162]
21. Fujita-Becker S, Durrwang U, Erent M, Clark RJ, Geeves MA, Manstein DJ. Changes in Mg2+ ion concentration and heavy chain phosphorylation regulate the motor activity of a class I myosin. J Biol Chem. 2005; 280:6064–6071. [PubMed: 15579903]
22. Kintses B, Gyimesi M, Pearson DS, Geeves MA, Zeng W, Bagshaw CR, Malnasi-Csizmadia A. Reversible movement of switch 1 loop of myosin determines actin interaction. EMBO J. 2007; 26:265–274. [PubMed: 17213877]
23. Jacobs DJ, Trivedi D, David C, Yengo CM. Kinetics and thermodynamics of the rate-limiting conformational change in the actomyosin V mechanochemical cycle. J Mol Biol. 2011; 407:716–730. [PubMed: 21315083]
24. Trivedi DV, David C, Jacobs DJ, Yengo CM. Switch II Mutants Reveal Coupling between the Nucleotide- and Actin-Binding Regions in Myosin V. Biophys J. 2012; 102:2545–2555. [PubMed: 22713570]
25. Sun M, Oakes JL, Ananthanarayanan SK, Hawley KH, Tsien RY, Adams SR, Yengo CM. Dynamics of the upper 50-kDa domain of myosin V examined with fluorescence resonance energy transfer. J Biol Chem. 2006; 281:5711–5717. [PubMed: 16377637]
26. Yengo CM, Takagi Y, Sellers JR. Temperature dependent measurements reveal similarities between muscle and non-muscle myosin motility. J Muscle Res Cell Motil. 2012; 33:385–394. [PubMed: 22930330]
27. Sun M, Rose MB, Ananthanarayanan SK, Jacobs DJ, Yengo CM. Characterization of the pre-force-generation state in the actomyosin cross-bridge cycle. Proc Natl Acad Sci USA. 2008; 105:8631–8636. [PubMed: 18552179]
28. Pardee JD, Spudich JA. Purification of muscle actin. Methods Cell Biol. 1982; 24:271–289. [PubMed: 7098993]
29. Johnson KA. Rapid kinetic analysis of mechanochemical adenosinetriphosphatases. Methods Enzymol. 1986; 134:677–705. [PubMed: 2950300]
30. Muretta JM, Kyrychenko A, Ladokhin AS, Kast DJ, Gillispie GD, Thomas DD. High-performance time-resolved fluorescence by direct waveform recording. Rev Sci Instrum. 2010; 81:103101. [PubMed: 21034069]
31. Kast D, Espinoza-Fonseca LM, Yi C, Thomas DD. Phosphorylation-induced structural changes in smooth muscle myosin regulatory light chain. Proc Natl Acad Sci USA. 2010; 107:8207–8212. [PubMed: 20404208]

32. De La Cruz EM, Sweeney HL, Ostap EM. ADP inhibition of myosin V ATPase activity. Biophys J. 2000; 79:1524–1529. [PubMed: 10969013]
33. Kron SJ, Toyoshima YY, Uyeda TQ, Spudich JA. Assays for actin sliding movement over myosin-coated surfaces. Methods Enzymol. 1991; 196:399–416. [PubMed: 2034132]
34. Meijering E, Dzyubachyk O, Smal I. Methods for cell and particle tracking. Methods Enzymol. 2012; 504:183–200. [PubMed: 22264535]
35. De La Cruz EM, Wells AL, Rosenfeld SS, Ostap EM, Sweeney HL. The kinetic mechanism of myosin V. Proc Natl Acad Sci USA. 1999; 96:13726–13731. [PubMed: 10570140]
36. Rief M, Rock RS, Mehta AD, Mooseker MS, Cheney RE, Spudich JA. Myosin-V stepping kinetics: a molecular model for processivity. Proc Natl Acad Sci USA. 2000; 97:9482–9486. [PubMed: 10944217]
37. Robblee JP, Cao W, Henn A, Hannemann DE, De La Cruz EM. Thermodynamics of nucleotide binding to actomyosin V and VI: a positive heat capacity change accompanies strong ADP binding. Biochemistry. 2005; 44:10238–10249. [PubMed: 16042401]
38. Uemura S, Higuchi H, Olivares AO, De La Cruz EM, Ishiwata S. Mechanochemical coupling of two substeps in a single myosin V motor. Nat Struct Mol Biol. 2004; 11:877–883. [PubMed: 15286720]
39. Oguchi Y, Mikhailenko SV, Ohki T, Olivares AO, De La Cruz EM, Ishiwata S. Load-dependent ADP binding to myosins V and VI: implications for subunit coordination and function. Proc Natl Acad Sci USA. 2008; 105:7714–7719. [PubMed: 18509050]
40. Coureux PD, Wells AL, Menetrey J, Yengo CM, Morris CA, Sweeney HL, Houdusse A. A structural state of the myosin V motor without bound nucleotide. Nature. 2003; 425:419–423. [PubMed: 14508494]
41. Yengo CM, De la Cruz EM, Safer D, Ostap EM, Sweeney HL. Kinetic characterization of the weak binding states of myosin V. Biochemistry. 2002; 41:8508–8517. [PubMed: 12081502]
42. Nitta R, Okada Y, Hirokawa N. Structural model for strain-dependent microtubule activation of Mg-ADP release from kinesin. Nat Struct Mol Biol. 2008; 15:1067–1075. [PubMed: 18806800]
43. Dias CL, Ala-Nissila T, Wong-ekkabut J, Vattulainen I, Grant M, Karttunen M. The hydrophobic effect and its role in cold denaturation. Cryobiology. 2010; 60:91–99. [PubMed: 19616532]
44. Lopez CF, Darst RK, Rossky PJ. Mechanistic elements of protein cold denaturation. J Phys Chem B. 2008; 112:5961–5967. [PubMed: 18181599]
45. Fields PA. Review: Protein function at thermal extremes: balancing stability and flexibility. Comp Biochem Physiol A Mol Integr Physiol. 2001; 129:417–431. [PubMed: 11423314]
46. Romani A, Scarpa A. Hormonal control of Mg2+ transport in the heart. Nature. 1990; 346:841–844. [PubMed: 2168019]
47. Walter WJ, Koonce MP, Brenner B, Steffen W. Two independent switches regulate cytoplasmic dynein's processivity and directionality. Proc Natl Acad Sci USA. 2012; 109:5289–5293. [PubMed: 22411823]
48. Rosenfeld SS, Sweeney HL. A model of myosin V processivity. J Biol Chem. 2004; 279:40100–40111. [PubMed: 15254035]
49. Forgacs E, Cartwright S, Sakamoto T, Sellers JR, Corrie JE, Webb MR, White HD. Kinetics of ADP dissociation from the trail and lead heads of actomyosin V following the power stroke. J Biol Chem. 2008; 283:766–773. [PubMed: 17965414]

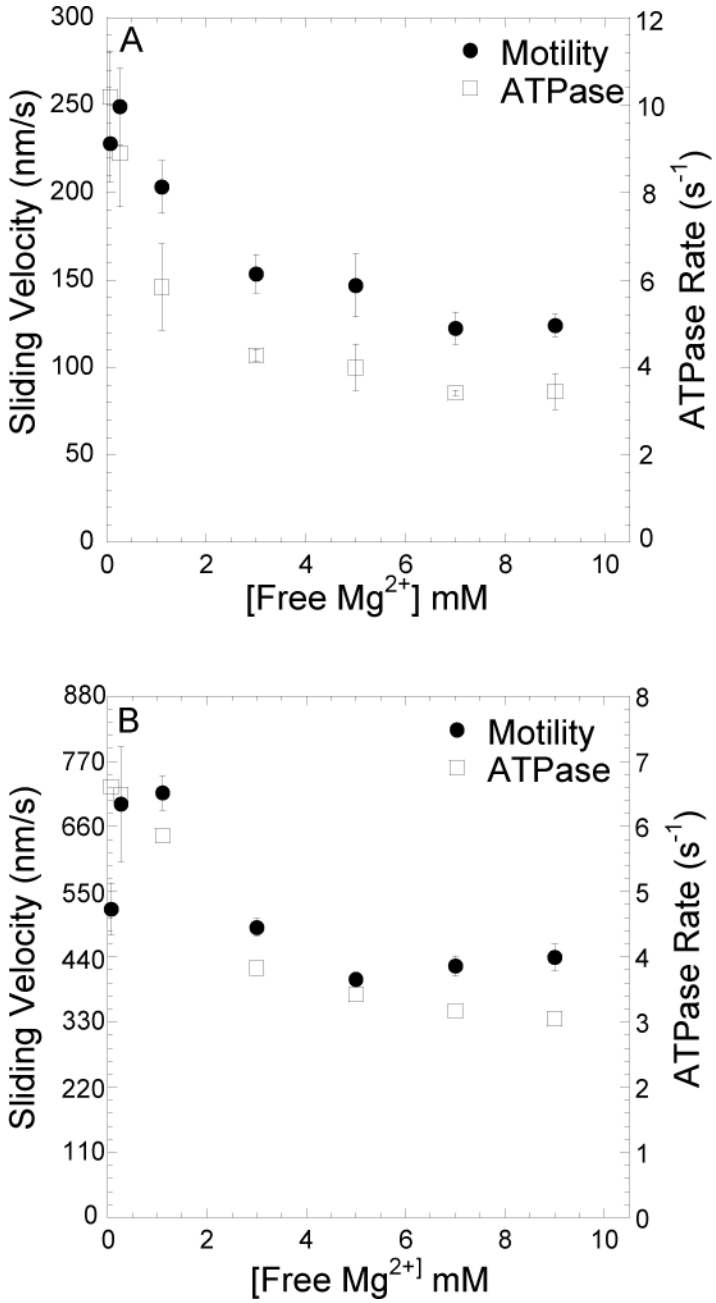

FIGURE 1. Steady-state ATPase and*in vitro*motility as a function of Mg

Steady state ATPase rate and *in vitro* motility of MV FlAsH (A) and MV HMM (B) was measured as a function of Mg concentration. The ATPase rates were measured with 20μM actin at 25°C using the NADH coupled assay. The *in vitro* motility sliding velocities were also measured as a function of Mg concentration (n = 20–30 filaments per Mg concentration). The data are plotted as a function of free Mg concentration. Error bars indicate SD for the ATPase measurements and SE for the motility measurements.

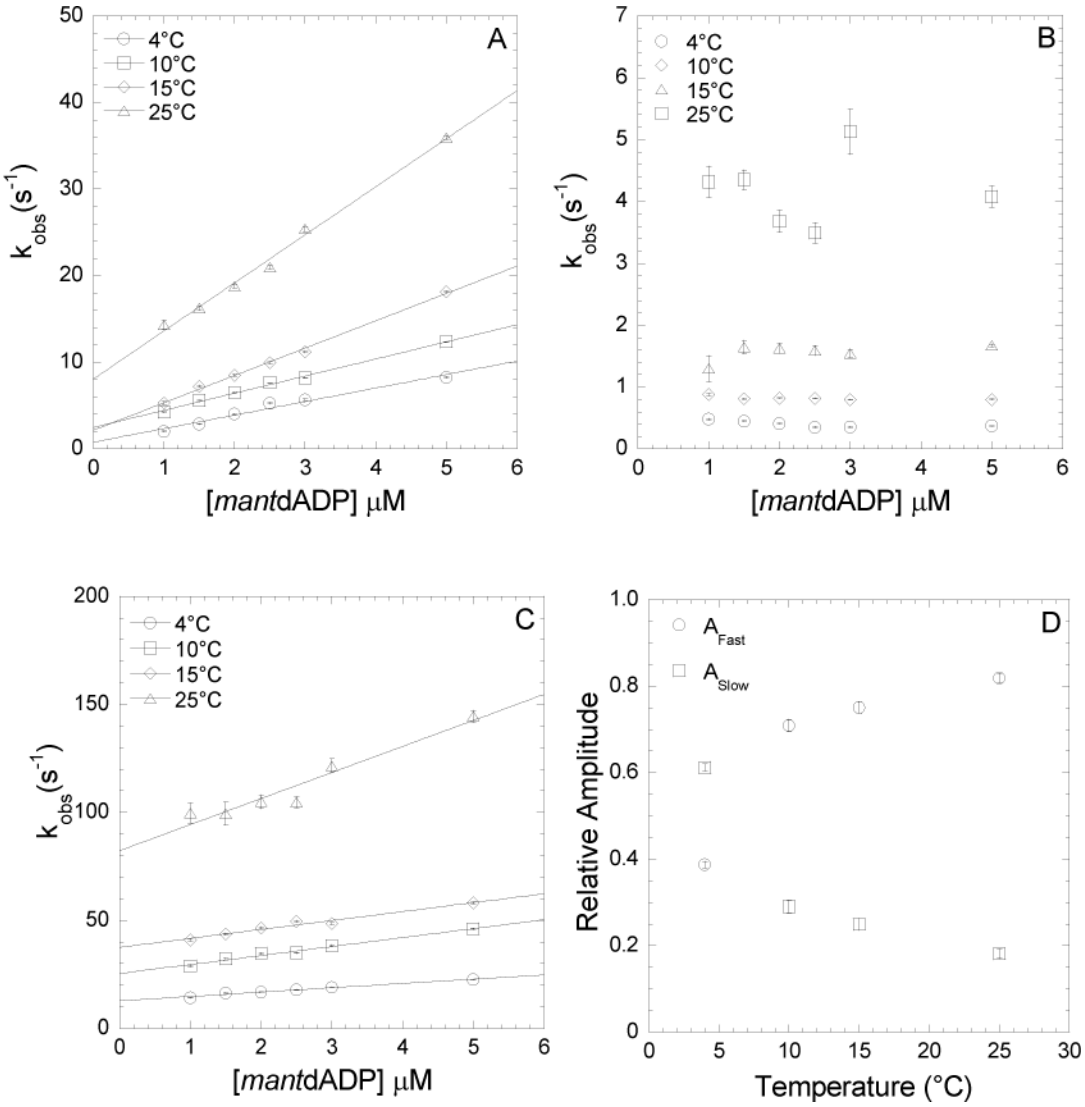

FIGURE 2. Kinetics of*mant*dADP binding to actomyosin V FlAsH in the presence and absence of Mg

Binding of *mant*dADP to actomyosin V FlAsH in the presence of 2mM $MgCl_2$ and 4mM EDTA was measured. In the presence of 2mM $MgCl_2$, fluorescence transients were bi-exponential with a fast and a slow phase while in the presence of 4mM EDTA, binding was single exponential with a single, fast phase. *A*, At 2mM $MgCl_2$, the ligand and temperature dependent fast phase was fit to a linear relationship to obtain a second-order binding constant at the indicated temperatures. *B*, At 2mM $MgCl_2$, the ligand independent and temperature dependent slow phase is plotted as a function of temperature. *C*, At 4mM EDTA, the ligand and temperature dependent fast phase was fit to a linear relationship. *D*, Relative amplitudes of the fast and slow phases at 2mM $MgCl_2$ are plotted as a function of temperature.

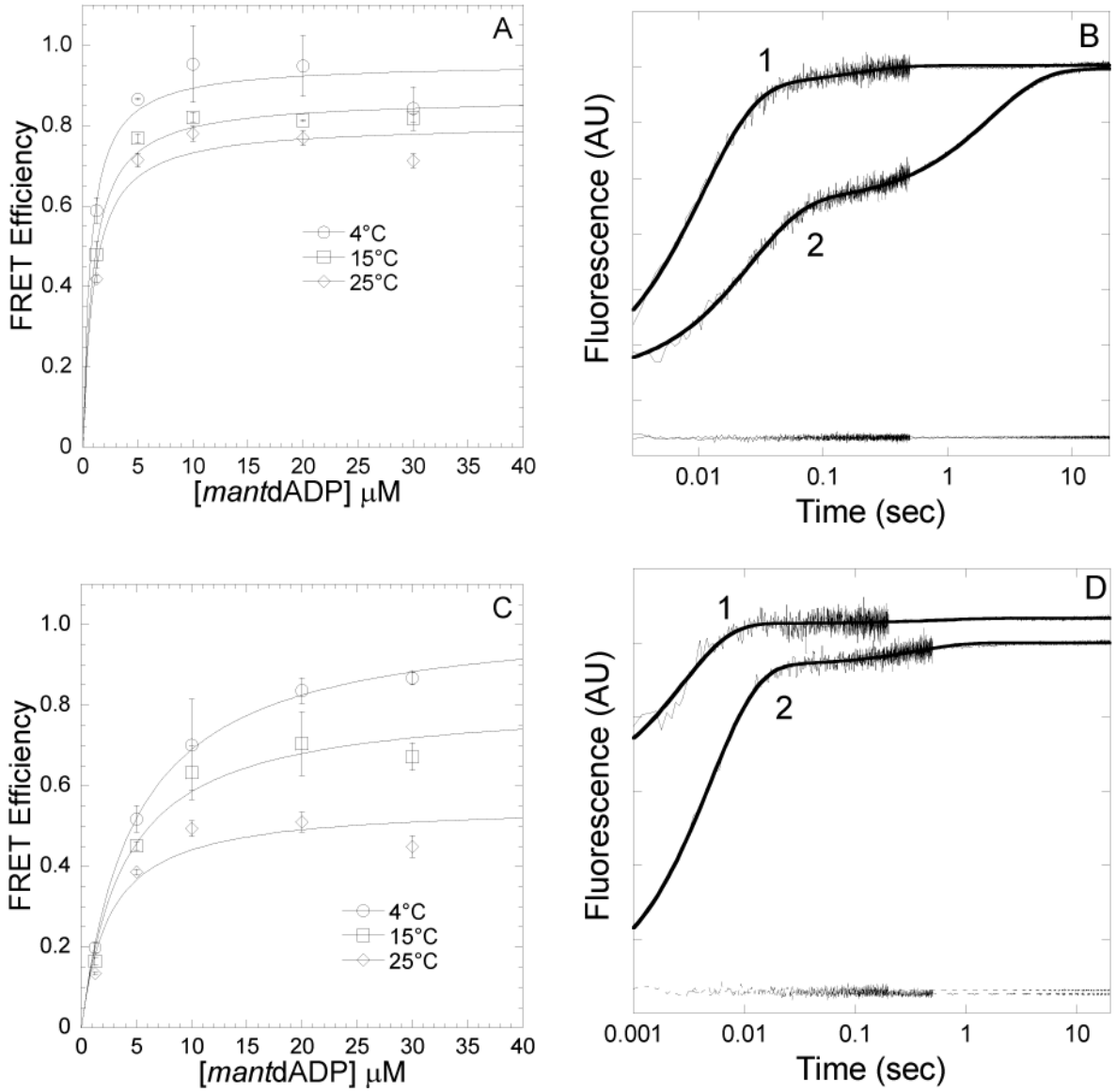

FIGURE 3. Conformation of the nucleotide binding pocket of acto-MV FlAsH as a function of Mg and temperature in the presence of *mant*dADP

FRET efficiency was determined in a stopped-flow by mixing acto-MV FlAsH with increasing concentrations of *mant*dADP and measuring the acceptor enhancement. The FRET efficiency was measured at 4, 15 and 25°C in the presence of 2mM $MgCl_2$(*A*) and 4mM EDTA (*C*). The data were fit to a hyperbolic binding function to determine the maximum FRET efficiency. Error bars indicate SD from at least two separate experiments done with at least two different protein preparations. Representative fluorescence traces of *mant*dADP (30μM) binding to actomyosin V FlAsH (0.25μM) in the presence of 4mM EDTA (*1*) or 2mM $MgCl_2$(*2*) at 4°C (*B*) or 25°C (*D*) are shown. The traces are fit to a double exponential function in all cases. The acceptor alone (actomyosin V FlAsH) traces are also shown at the bottom of the graph.

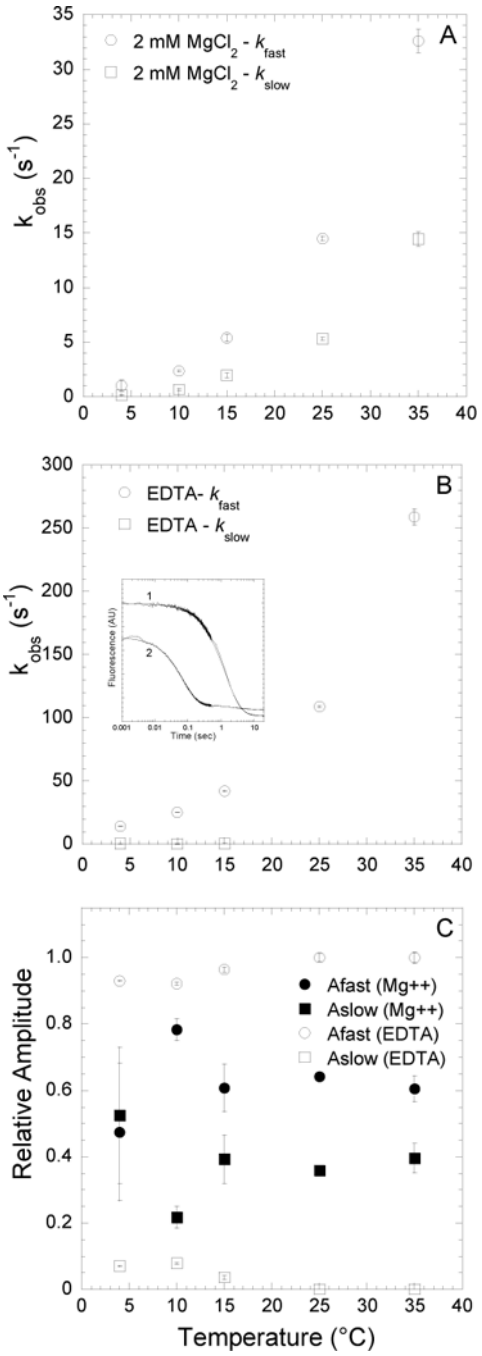

FIGURE 4. Kinetics of *mant*dADP dissociation from actomyosin V FlAsH in the presence and absence of Mg

Fluorescence transients were monitored by following the acceptor enhancement after actomyosin V FlAsH complexed with *mant*dADP was rapidly mixed with saturating ATP. *A*, At 2mM $MgCl_2$, the dissociation of *mant*dADP from actomyosin V FlAsH was fit to a double exponential function with the fast and slow phases plotted as a function of temperature. *B*, In the presence of 4mM EDTA, the fluorescence transients of *mant*dADP dissociation were fit to a double exponential function at lower temperatures (4–15°C) and single exponential function at higher temperatures (25–35°C). The fast and slow phases are plotted as a function of temperature. Inset shows representative fluorescence transients of

*mant*dADP dissociation in the presence of 2 mM $MgCl_2$ (trace 1) and 4 mM EDTA (trace 2) at 4°C plotted on a log scale and fit to a double exponential function. *C*, Relative amplitudes of the fast and slow phases, in the presence of 2mM $MgCl_2$ or 4mM EDTA are plotted as a function of temperature.

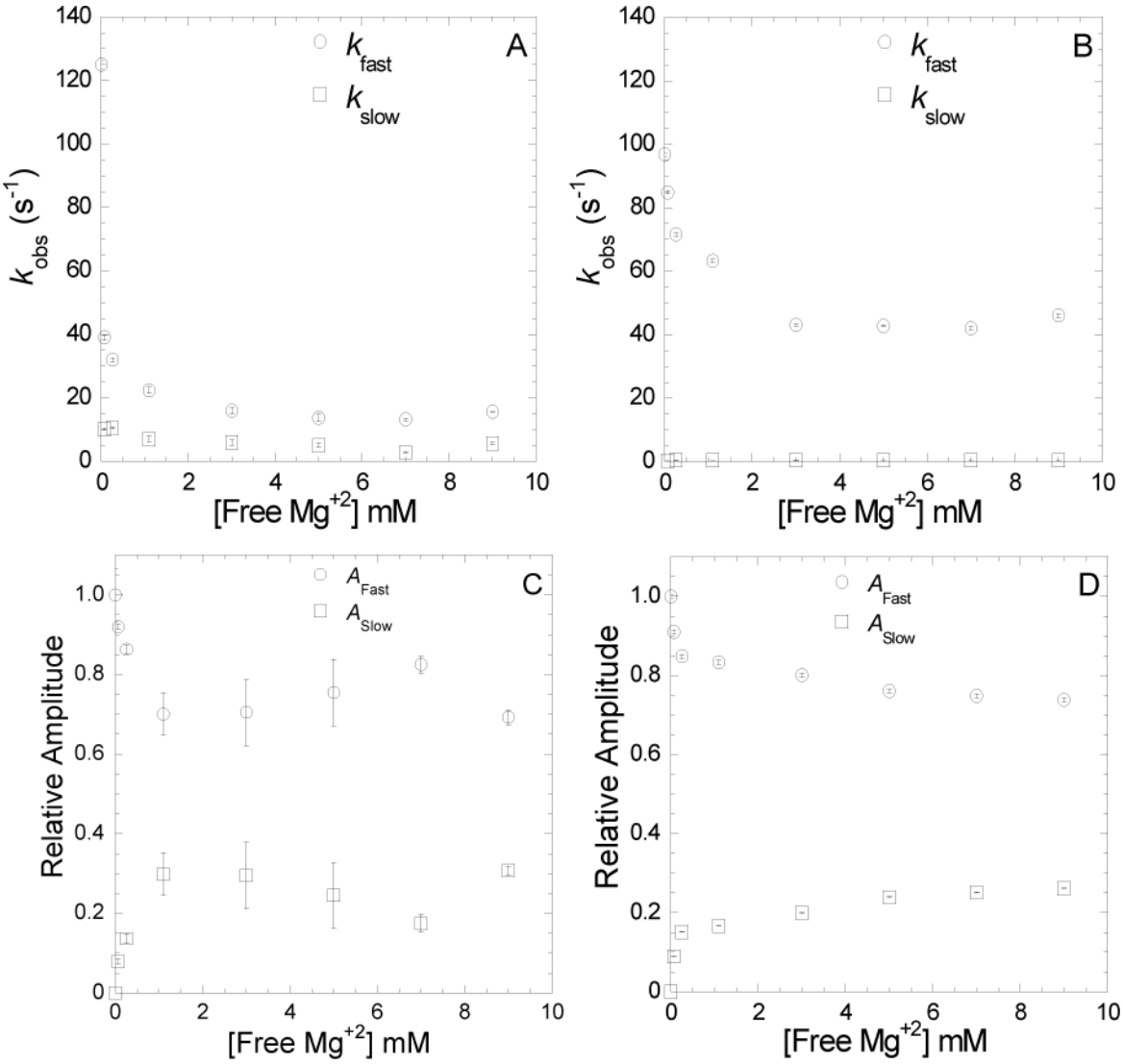

FIGURE 5. Impact of Mg concentration on the strong to weak transition of the NBP and release of *mant*dADP from the weak binding state

Dissociation of *mant*dADP from actomyosin V FlAsH, as described in Fig. 4, was measured at 25°C and varying free Mg concentrations. The slow and fast phases of *mant*dADP release from acto MV WT (*A*) or acto MV G440A (*B*) are plotted as a function of free Mg concentration. Relative amplitudes of the fast and slow phases of *mant*dADP release from FlAsH labeled acto-MV WT (*C*) or acto-MV G440A (*D*) are plotted as a function of free Mg concentration.

FIGURE 6

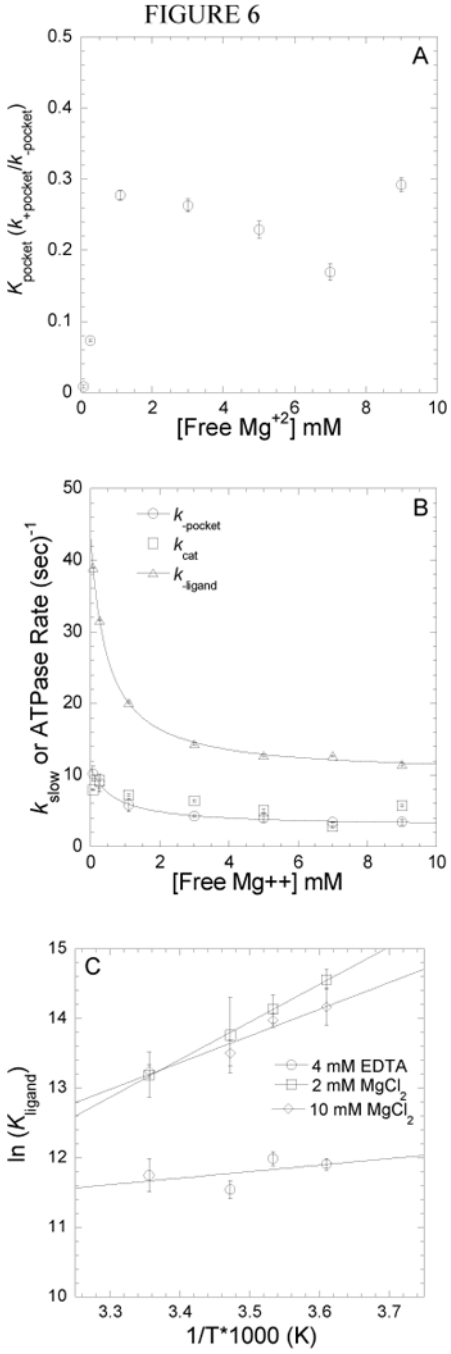

FIGURE 6. Correlation of the strong-to-weak transition of the NBP and the ATPase rate as a function of Mg

A, The equilibrium constant (K_{pocket}) of the strong-to-weak transition of the NBP is plotted as a function of free Mg. *B*, The rates of the NBP transitioning into the weak ADP binding state ($k_{-pocket}$), ligand release ($k_{-ligand}$) and the ATPase rate (k_{cat}) are plotted as a function of free Mg. There is a strong correlation between the rate limiting transition of the NBP into the weak ADP binding state and the ATPase rates at all free Mg concentrations. Data are fit to Eq. 14. *C*, The van't Hoff plots of K_{ligand} measured in the presence (2 mM and 10 mM $MgCl_2$) and absence of Mg (4 mM EDTA). The thermodynamic parameters are summarized in Table 3.

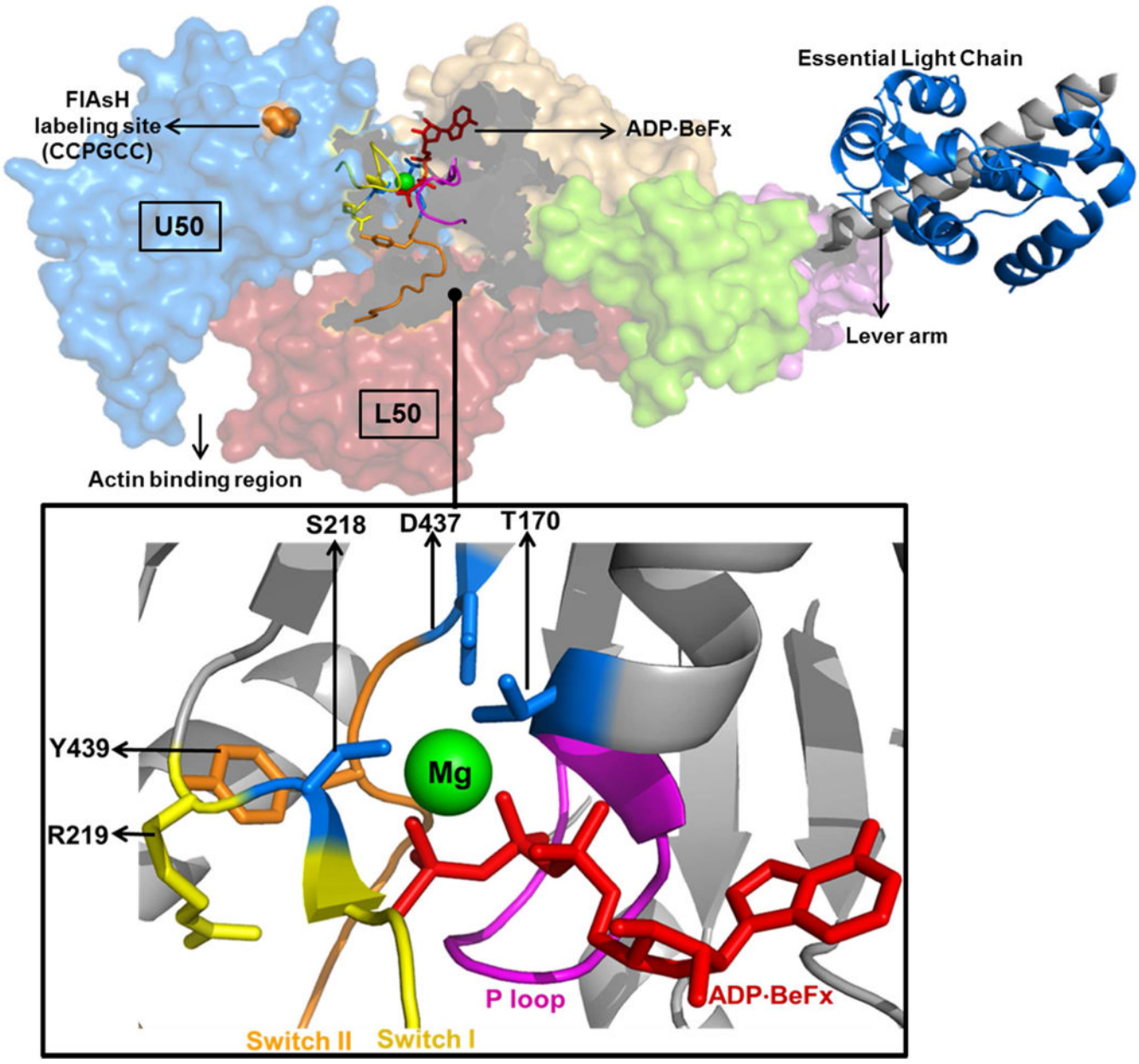

FIGURE 7. Structural details of Mg coordination

Crystal structure of Myosin V complexed with ADP-BeFx (top, PDB 1w7j) is shown. The actin and nucleotide binding regions are highlighted along with the upper and lower 50 kDa domains (U50 and L50 respectively). Proline of the FlAsH-binding tetracysteine motif (CC**P**GCC) is highlighted on the U50 domain. Key structural elements involved in Mg coordination are magnified (bottom) and described in the text.

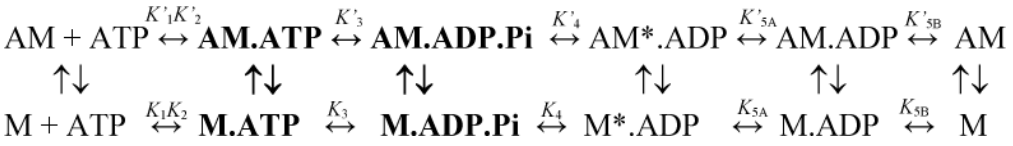

Scheme 1.

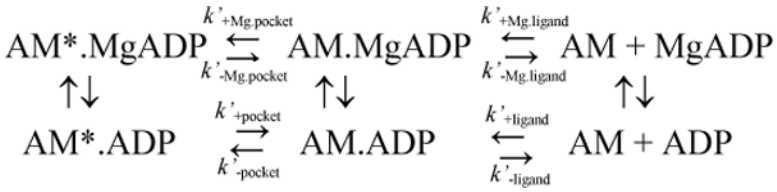

Scheme 2.

TABLE 1

Summary of *mantd*ADP binding to and release from acto-MV FlAsH in the presence (2 mM or 10 mM $MgCl_2$) and absence of Mg (4 mM EDTA).

Rate Constant	2 mM $MgCl_2$				10 mM $MgCl_2$			
	4°C	10°C	15°C	25°C	4°C	10°C	15°C	25°C
$k_{+ligand}$ ($\mu M^{-1} \bullet s^{-1}$)	1.56±0.13	2.65±0.05	3.16±0.09	5.55±0.23	1.21±0.07	2.00±0.11	2.49±0.15	4.72±0.21
$^{a}k_{-ligand}$ (s^{-1}) y-intercept	0.79±0.36	1.65±0.13	2.17±0.25	8.08±0.6	1.00±0.21	1.76±0.30	3.84±0.41	8.80±0.60
$k_{-ligand}$ (s^{-1})	0.70±0.20	1.70±0.01	4.50±0.10	12.60±0.10	0.68±0.01	1.59±0.01	3.04±0.01	7.86±0.03
$1/K_{ligand}$ (μM)	0.47±0.07	0.73±0.15	1.06±0.52	1.86±0.58	0.70±0.18	0.85±0.08	1.37±0.24	1.77±0.16
$k_{+pocket}$ (s^{-1})	0.24±0.15	0.19±0.02	0.74±0.39	1.33±0.91	0.11±0.01	0.37±0.29	0.40±0.08	0.74±0.43
$k_{-pocket}$ (s^{-1})	0.51±0.34	0.85±0.12	2.22±0.28	5.79±0.20	0.37±0.03	0.94±0.22	1.55±0.70	3.99±2.24
$K_{pocket} = k_{+pocket}/k_{-pocket}$	0.47±0.43	0.23±0.04	0.33±0.18	0.23±0.16	0.28 ±0.03	0.40 ±0.32	0.26±0.13	0.19±0.15
$^{b}K_D$ (μM)	0.32±0.30	0.87±0.28	0.64±0.39	1.32±0.92	0.54±0.15	0.61±0.36	1.09±0.57	1.54±1.24
$^{c}K_D$ (μM)	0.70±0.26	ND	0.92±0.16	0.98±0.32	ND	ND	ND	ND

Rate Constant	4 mM EDTA			
	4°C	10°C	15°C	25°C
$k_{+ligand}$ ($\mu M^{-1} \bullet s^{-1}$)	2.01±0.14	4.15±0.27	4.14±0.38	12.06±1.61
$k_{-ligand}$ (s^{-1}) y-intercept	12.85±0.41	25.52±1.06	37.63±1.06	82.35±4.52
$k_{-ligand}$ (s^{-1})	14.1±0.1	25.3±0.2	42.2±0.6	108.9±0.8
$1/K_{ligand}$ (μM)	6.75±0.54	6.24±0.61	9.73±1.23	7.90±1.87
$k_{+pocket}$ (s^{-1})	ND	ND	ND	ND
$k_{-pocket}$ (s^{-1})	ND	ND	ND	^{d}14.77 ±2.00
$K_{pocket} = k_{on}/k_{off}$	ND	ND	ND	ND
$^{c}K_D$ (μM) (Fig. 3)	4.87±0.33	ND	3.87±1.01	2.55±1.17

[a] determined from the y-intercept of the linear fits in Figure 2

[b] calculated with equation 7

[c] determined from the hyperbolic fits in Figure 3

[d] determined from the fit of the data in Figure 6B (extrapolated to Mg-free conditions)

TABLE 2

Temperature dependent FRET results for acto-MV FlAsH bound to *mant*dADP in the presence (2 mM $MgCl_2$) and absence of Mg (4 mM EDTA).

Condition	4°C		15°C		25°C	
	FRET efficiency	[a] r (Å)	FRET efficiency	[a] r(Å)	FRET efficiency	[a] r (Å)
2 mM $MgCl_2$	0.96±0.04	15.5 (10.3–17.4)	0.87±0.02	18.6 (18.1–19.2)	0.81±0.04	20.0 (19.1–20.7)
4 mM EDTA	0.99±0.02	12.5 (12.5–15.0)	0.81±0.05	20.9 (19.6–21.9)	0.55±0.05	24.9 (24.1–25.7)

[a] errors are reported as a range of distances in parentheses

TABLE 3

Thermodynamic parameters as a function of Mg.

Equilibrium Constant	ΔG (kcal/mole)	ΔH (kcal/mole)	ΔS (cal/mole•°K)	TΔS (kcal/mole)
K_{ligand} (EDTA)	−7.0±0.1	−1.9±2.2	17.1±7.4	5.1±2.2
K_{ligand} (2 mM Mg)	−7.9±0.1	−10.7±0.4	−9.7±1.4	−2.9±0.4
K_{ligand} (10 mM Mg)	−7.8±0.1	−7.6±1.4	0.8±4.5	0.2±1.3
K_{pocket} (2 mM Mg)	0.9±0.5	−4.4±3.3	−17.8±11.2	5.3±3.3
K_{pocket} (10 mM Mg)	1.0±0.6	−4.2±2.8	−17.4±9.8	5.2±2.9

TABLE 4

Time-resolved anisotropy parameters of the FlAsH fluorophore.

Parameters	AMV FlAsH. ADP	AMV FlAsH
Lifetime 1 (ns)	5.43±0.01	5.41±0.01
Relative Amplitude	0.9	0.9
Maximum Anisotropy	0.33±0.01	0.33±0.01
Final Anisotropy	0.17±0.03	0.17±0.03
Correlation Time (ns)	8.28±1.54	8.24±1.40
Lifetime 2 (ns)	0.73±0.01	0.73±0.01
Relative Amplitude	0.1	0.1